Principle and applications of Controlled-Drift Detectors

A.Castoldi [a,1] C.Guazzoni [b] R.Hartmann [c] L.Strüder [d]

[a] *Dip. Ingegneria Nucleare Ce.S.N.E.F., Politecnico di Milano, P.za Leonardo da Vinci 32, 20133 Milano, Italy and INFN, Sez. di Milano*

[b] *Dip. Elettronica e Informazione, Politecnico di Milano, P.za Leonardo da Vinci 32, 20133 Milano, Italy and INFN, Sez. di Milano*

[c] *PNSensor GmbH, Römer Strasse 28, D-80803 München, Germany*

[d] *Max Planck Institut für Extraterrestriche Physik, Otto-Hahn-Ring 6, D-81739 München, Germany*

Abstract

The Controlled-Drift Detector is a fully-depleted silicon detector that allows 2-D position sensing and energy spectroscopy of X-rays in the range $0.5 - 30keV$ with excellent time resolution (few tens of μs) and limited readout channels. In this paper we review the Controlled-Drift Detector operating principle and we present some applications of Controlled-Drift Detectors in X-ray absorption imaging and in Compton electrons tracking.

Key words: Controlled-Drift Detectors, X-ray imaging, X-ray spectroscopy, Compton imaging

1 Introduction

The Controlled Drift Detector (CDD) is the more recent evolution of silicon drift detectors [1,2] for 2D position sensing and spectroscopy of X-rays. It operates in single-photon counting mode and features position-sensing capability of the order of $100\mu m$, energy resolution comparable to spectroscopic-grade silicon drift detectors and event timing better than $10ns$. Frame rates up to 125 kHz have been successfully tested when operated in integrate-readout mode.

[1] Corresponding author: Tel.: +39 02 2399 6321; fax: +39 02 23996309.
E-mail address: Andrea.Castoldi @ polimi.it

In this paper we will review the CDD working principle and focus on two promising fields of application (X-ray absorption imaging and Compton electrons tracking).

2 CDD operating principle

The Controlled Drift Detector (CDD) [3,4] is a new silicon detector topology proposed in 1997 that allows position sensing and spectroscopy of each detected X-ray with readout times of few microseconds. Full depletion of the $300 - 450\mu m$-thick Silicon substrate allows direct detection of X-rays with good efficiency up to 30 keV. The specially tailored entrance window on the back side sets the lower threshold for the detection efficiency below $1keV$ (sensitivity down to the 277 eV Carbon line has been demonstrated) [6]. The detector can be operated in integrate-readout mode or in continuous readout mode. In integrate-readout mode the CDD features a typical full frame duration (exposure plus readout) of few tens of μs [4,5]. In this operating mode equally spaced potential wells are generated along the drift direction by superposing an externally controllable perturbation to the linear drift potential. On-chip n-channel JFETs allow low noise measurement of the drift time and of the total charge of each electron packet which provide, respectively, the position information along the drift coordinate and the X-ray energy. The segmentation of the anodes gives the second orthogonal coordinate. Pixel size down to $120\mu m$ has been successfully tested [8]. The electron transport takes place at about $7 - 8\mu m$ from the front surface within a high-energy n-type implanted layer. In order to improve electron transport during the drift mode, properly tailored deep n-implants along the drift direction have been recently added [7]. Measured drift velocities are in the range $0.2 - 0.5cm/\mu s$ leading to readout times of $2 - 5\mu s$ for a 1-cm-long detector. Based on the relatively fast electron drift velocity in silicon, the integrate-readout cycle of a CDD can be therefore as short as few tens of μs which is significantly shorter than the one of a Charge-Coupled Device [9] with parallel column readout. The benefits of a shorter integration time are the possibility to operate the CDD at room temperature still having an acceptable energy resolution and the better capability of time-resolved imaging. The best measured energy resolution at the Mn $K\alpha$ line ($5.9keV$) is about $270eV FWHM$ at room temperature [10] with a small-area prototype ($2mm$ drift length - $180\mu m$ pixel size). With a medium-area prototype ($6mm$ drift length - $180\mu m$ pixel size) the energy resolution was limited to $1.2keV$ $FWHM$ at the $13.9keV$ Np $L\alpha$ line at room temperature, due to an excess of leakage current of the prototype under test. By moderately cooling down the detector ($T = 240K$) the energy resolution improves to $300eV\,FWHM$ and the drift time from the farthest pixel reduces

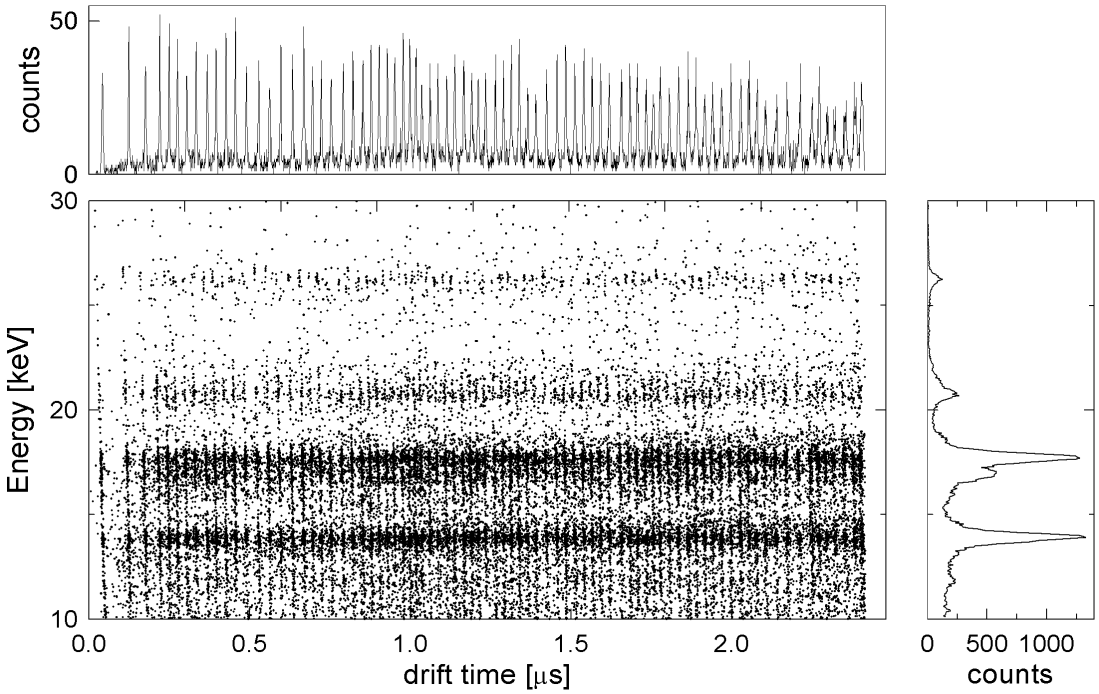

Fig. 1. Scatter plot energy vs drift time of the X-rays of a ^{241}Am source collected by irradiating a column of the CDD at 67 kHz frame frequency (T=300K). The upper inset shows the distribution of the events along the time axis. The inset on the right end shows the total distribution of the event energies (i.e. the spectrum of the ^{241}Am source collected by all the pixels).

to $0.8\mu s$, thus allowing the operation of the detector at $125kHz$ frame rate. We have carried out preliminary spectroscopic tests with the novel large-area prototype (240 drifting columns with $10.2mm$ drift length and $120\mu m$ pixel size) at room temperature. The detector was irradiated with a ^{241}Am radioactive source. Fig. 1 shows the scatter plot energy vs. drift time (i.e. position) of the events detected by a single column when the CDD is operated at 67 kHz frame rate. Moving along the time axis we see that the events are gathered in well separated clusters centered at the characteristics lines of the ^{241}Am source and indicating the illuminated pixels. The upper inset of Fig. 1 shows the distribution of the events along the time axis. The FWHM of the peaks is about 26% which further reduces at lower drift fields allowing reduction of the pixel size. The inset on the right end of Fig. 1 shows the total distribution of the event energies (i.e. the spectrum of the ^{241}Am source collected by all the pixels in the column). The energy resolution at the Np $L\alpha$ line ($13.9keV$) is $530eV\,FWHM$, corresponding to an Equivalent Noise Charge (ENC) of 59 electrons r.m.s.. We expect that the resolution can drop below $200eV\,FWHM$ by Peltier cooling the detector.

The p+ back electrodes are instrumented to pick-up the fast induction pulse of the signal electrons and holes. During the initial carrier separation a unipolar current pulse, lasting few nanoseconds (depending on substrate resistivity and on the ionization profile), is induced on the p+ back electrode that collects the holes. A time resolution of $3.5ns\,FWHM$ has been measured in the case of injection of $30,000$ electrons with an infrared (904 nm) laser pulse

Fig. 2. X-ray radiographic image of a lizard acquired with a CDD operated at $100kHz$ frame frequency ($300K$). The image is obtained accumulating $150,000$ frames. The energy of the incident beam was set to $15keV$. The darker the pixel in the gray scale, the lower the number of counts in the pixel.

[11]. Coincidence measurements carried out using a fast scintillator-PMT as the time reference and the annihilation photons of a ^{22}Na source showed an overall resolution (including the statistics of the generation process) of 6 ns FWHM [12]. In the second operating mode, i.e. continuous readout, the pick-up signal from the back electrodes (or an external trigger if available) is used as the start of the electrons' drift to measure the drift coordinate.

3 X-ray absorption imaging

Fig. 2 shows the X-ray image of a lizard obtained accumulating 150,000 frames at 100 kHz. The energy of the incident beam was set to 15 keV, high enough to pass through the lizard organs. Due to the small dimensions of this prototype, the detector was panned to cover the whole imaged area. The details in the lizard body, are beautifully resolved. Not only the vertebral column and the rib bones can be clearly distinguished but also a faint image of the lungs is obtained. The two black spots in the radiography are due to two small stones that were present inside the lizard body. The abrupt change of the X-ray refractive index, e.g. at the edges between the lizard body and air, is responsible for the sharp enhancement of the image due to scattering of the collimated X-ray beam and large sample to detector distance (about $1.5m$ in our case). If needed the information about the energy spectrum of the photons collected in each pixel of the digital radiography is available. This feature can be used to exclude inelastic scattered photons that can spoil the contrast of the acquired image or to apply energy cuts.

4 Compton electrons tracking

The excellent energy resolution of low capacitance drift detectors and the relatively small Doppler broadening of silicon [13] make CDDs suitable candidates as scatter detectors in Compton telescopes with angular resolution of the order of 1 degree or better for a wide range of gamma ray energies. This is of particular interest in the field of small-animal SPECT for in-vivo study of radiopharmaceuticals distribution. The fact that the charge packets are drifted to one side of the detector chip gives the additional advantage of a reduced number of output channels and of the possibility to stack several silicon layers with reduced amount of mass along the photon path. The signals induced on the back electrodes by the initial motion of the electron-hole track generated by the recoil electron generate the fast trigger needed for event coincidence.

4.0.1 Theoretical background

In a Compton telescope the direction of the incident γ-ray is constrained to lie on a cone with aperture θ and axis given by the measured direction of the scattered photon [14]. The estimation of the direction of the recoil electron at the first Compton interaction allows reducing the event circle to a short arc which significantly increases the sensitivity of the Compton telescope. However, in present telescopes this possibility, if present, is limited to high energy electrons that cross more detection layers. The good energy resolution of Controlled-Drift Detectors joined with their pixellated structure allows recording the electron track within a single interaction layer and therefore imaging electron tracks also for low energy electrons, often totally absorbed in the interaction layer owing to the short electron range [15]. This would be an essential upgrade not only in the case of low gamma energies ($\leq 0.5MeV$) as it also improves background rejection and event reconstruction. The CDD records the 2D projection of the electron track and its ionization profile by sampling the charge fraction deposited in each pixel. The projection of the initial direction of the recoil electron, the vertex of the interaction and the electron energy can therefore be more precisely estimated for wide range of Compton electron energies leading to improved resolution and efficiency. For the electrons that escape from a single silicon layer the comparison of the data with the known theoretical curve (dE/dx versus E) allows us to derive a least-square estimate of the recoil electron energy (T_e) and of the escape energy. The lack of the Depth-Of-Interaction (DOI) information affects the estimation of dE/dx and limits the accuracy of this analysis. It must be pointed out however that the shape of the induced signals on segmented back electrodes could also be used to provide DOI information at the expense of a more sophisticated signal processing.

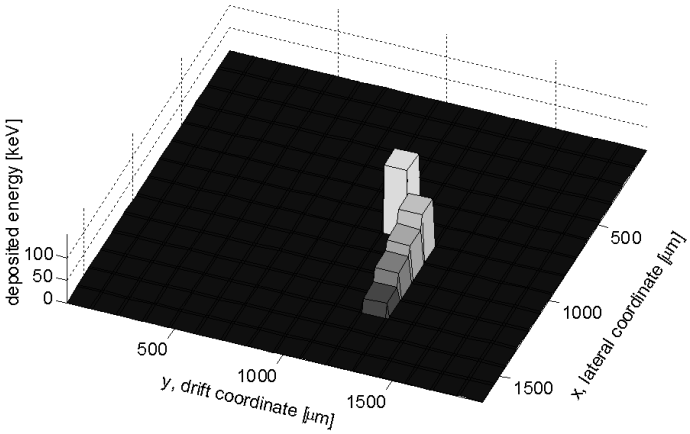

Fig. 3. Example of recorded Compton electron tracks originated by γ-rays coming from a ^{22}Na source

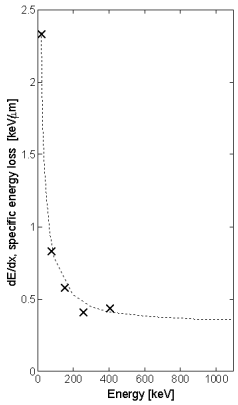

Fig. 4. Estimated specific energy loss after least-square-fit to the theoretical curve (solid line). The measured Compton electron energy is $407keV$

4.1 Experiment

A small-area detector prototype having 13 $120\mu m$-wide drift channels was operated at room temperature in continuous readout mode and irradiated with a ^{22}Na source to image Compton electron tracks. The induction signal picked up at the uniform back contact provided the interaction time (and the start of the electron drift) with a measured time jitter of about $6ns\,FWHM$. Fig. 3 shows an example of an electron track fully absorbed in the silicon layer. Pixel height corresponds to the deposited energy (in keV). Fig. 4 shows the estimated specific energy loss after least-square-fit to the theoretical curve (solid line). Although more refined data analysis can be performed this result already show how these detectors can add direct 'true imaging' capability to Compton telescopes which is an attractive way to increase their sensitivity and spatial resolution.

References

[1] E.Gatti, P.Rehak, *Nucl. Instr. and Meth.* A225 (1984), 608.

[2] A.Castoldi, P.Rehak, and P.Holl, *Nucl. Instr. and Meth.* A377 (1996) 375.

[3] E.U. Patent n. EP0862226 , US Patent n. US 6,249,033

[4] A.Castoldi, C.Guazzoni, E.Gatti, A.Longoni, P.Rehak, L.Strüder, *IEEE Trans. Nucl. Sci.* 44 (1997) 1724.

[5] A.Castoldi, G.Cattaneo, A.Galimberti, C.Guazzoni, P.Rehak, L.Strüder, *IEEE Trans. Nucl. Sci.* 49 (2002) 989.

[6] R.Hartmann, K.H.Stephan, L.Strüder, *Nucl. Instr. Meth.* A439 (2003) 216.

[7] A.Castoldi, C.Guazzoni, L.Strüder, *IEEE Trans. Nucl. Sci.* 49 (2002) 1055.

[8] A.Castoldi, A.Galimberti, C.Guazzoni, P.Rehak, L.Strüder, *Nucl. Instr. Meth.* A518 (2004) 426.

[9] L.Strüder et al., *Rev. Sci. Instrum.* 68 (1997) 4271.

[10] A.Castoldi, C.Guazzoni, P.Rehak, L.Strüder, *IEEE Trans. Nucl. Sci.* 48 (2001) 982.

[11] A. Castoldi, E. Gatti, C. Guazzoni, *Nucl. Instr. and Meth.* A518, (2004) 429.

[12] A. Castoldi, A. Galimberti, C. Guazzoni, L.Strüder, A. H. Walenta, in press on *IEEE . Trans. Nucl. Sci.*, 2006

[13] C.E.Ordonez, A.Bolozdynya, W.Chang, *Proc. of the IEEE Nuclear Science Symposium* (1997) 1361.

[14] T. Conka-Nurdan, K. Nurdan, F. Constantinescu, B. Freisleben, N.A. Pavel, A.H. Walenta, *IEEE Trans. Nucl. Sci.* 49(3), 2002, 817.

[15] O'Neill TJ, Ait-Ouamer F, Schwartz I, Tumer OT, White RS, Zych AD, *IEEE . Trans. Nucl. Sci.* 39 (1992) 629.